Raman study of oxygen reduced and re-oxidized strontium titanate

D. A. Tenne[*]

Department of Physics, Pennsylvania State University, University Park, Pennsylvania 16802, USA
and Department of Physics, Boise State University, Boise, Idaho 83725-1570, USA

I. E. Gonenli, A. Soukiassian, and D. G. Schlom

Department of Materials Science and Engineering, Pennsylvania State University, University Park, Pennsylvania 16802, USA

S. M. Nakhmanson[†] and K. M. Rabe

Department of Physics and Astronomy, Rutgers, State University of New Jersey, Piscataway, New Jersey 08854–8019, USA

X. X. Xi

Department of Physics, Department of Materials Science and Engineering, and Materials Research Institute,
Pennsylvania State University, University Park, Pennsylvania 16802, USA

We report Raman study of oxygen reduced single crystal strontium titanate. Oxygen reduction leads to the appearance of the forbidden first-order Raman peaks, as well as spectral features attributed to the local vibrational modes associated with oxygen vacancies. This assignment is supported by *ab initio* calculations of phonon modes in $SrTiO_3$ with introduced oxygen vacancies. Raman studies of re-oxidized samples show the same spectra as the initial single crystals. Comparison of Raman spectra of $SrTiO_3$ thin films and reduced $SrTiO_3$ single crystals demonstrates the importance of other factors such as polar grain boundaries in the lattice dynamical behavior of thin films.

I. INTRODUCTION

Strontium titanate ($SrTiO_3$) has been one of the most intensively studied perovskite oxide materials.[1] Recently, thin film $SrTiO_3$ and $Ba_xSr_{1−x}TiO_3$ have been the subject of many studies because of their potential for device applications, such as dynamic random access memory or tunable microwave devices.[2–4] An issue of major importance for device applications of these materials has been the understanding of the difference between thin film and bulk crystal behaviors, in particular, the specific lattice dynamical properties of thin films. Lattice dynamics is essential for understanding the fundamental properties of ferroelectrics, since the optical phonon frequencies are related to the static dielectric constant and ferroelectric and structural phase transitions. Recent studies of $SrTiO_3$ (Refs. 5–7) and $Ba_xSr_{1−x}TiO_3$ (Refs. 8–12) thin films revealed essential differences in their lattice dynamical properties compared to bulk crystals. In particular, the first-order Raman scattering, which is symmetry forbidden in paraelectric cubic perovskites, was observed in thin film $SrTiO_3$,[6,7] which is an incipient ferroelectric[13] and remains in a paraelectric phase down to 0 K. In $Ba_xSr_{1−x}TiO_3$ films, first-order Raman modes were observed well above the bulk ferroelectric-paraelectric phase transition temperature.[8,9,11] Significant hardening of the soft phonon modes in $SrTiO_3$ and $Ba_xSr_{1−x}TiO_3$ films, compared to bulk crystals was also observed.[5,7–9,11] These specific lattice dynamical properties of thin films were attributed to the presence of polar nanoregions, existing in the films even at temperatures corresponding to the paraelectric phase in bulk.[6–9]

Several possible causes for the formation of the polar nanoregions in ferroelectric thin films were suggested. In polycrystalline $SrTiO_3$ films, Ostapchuk *et al.*[14] observed defects such as porosity and cracks along the grain boundaries and suggested these defects to cause the appearance of symmetry-forbidden Raman peaks and soft mode hardening. However, these defects were not found in epitaxial films studied by Xi and co-workers,[5–7] as demonstrated by Wu *et al.*[15] Another cause for the appearance of polar nanoregions proposed by Petzelt *et al.*[16] for $SrTiO_3$ ceramics is the presence of dipoles localized at the grain boundaries, which can explain the observed soft mode hardening and the presence of the symmetry-forbidden first-order Raman peaks in the spectra of epitaxial $SrTiO_3$ films. Other factors that can cause thin film properties to be different from bulk include nonstoichiometry, inhomogeneous strain distribution, impurities, and oxygen vacancies, which are among the most common defects in oxide thin films.[17] Uwe *et al.* have shown that introducing oxygen vacancies into a nominally pure $SrTiO_3$ crystal leads to the appearance of local regions of ferroelectric polarization.[18] Infrared reflectance studies of highly reduced $SrTiO_3$ showed the presence of oxygen vacancies to cause hardening of the TO phonon.[19] It is important to know which of these factors plays a more significant role in determining the thin film behavior.

In order to investigate the effect of oxygen vacancies on the lattice dynamics of $SrTiO_3$, we have studied oxygen reduced $SrTiO_3$ single crystals by Raman spectroscopy. We have found that the introduction of oxygen vacancies does lead to the appearance of the symmetry-forbidden first-order Raman peaks in the spectra of $SrTiO_3$. However, other features appear in the spectra as well, which are attributed to the local vibrational modes associated with oxygen vacancies. This assignment is confirmed by *ab initio* calculations of phonon modes in $SrTiO_3$ with introduced oxygen vacancies,

which show the appearance of phonon modes at frequencies absent in stoichiometric bulk SrTiO$_3$, but present in the spectra of heavily reduced SrTiO$_3$. Raman studies of re-oxidized samples (previously reduced SrTiO$_3$ annealed in oxygen atmosphere to decrease the number of oxygen vacancies) show the same spectra as initial single crystals, demonstrating that the observed spectral changes are indeed caused by oxygen reduction.

II. EXPERIMENTAL DETAILS

For the preparation of oxygen reduced SrTiO$_3$, commercially available single crystalline (001) SrTiO$_3$ substrates (CrysTec GmbH.) with the size $5 \times 5 \times 0.4$ mm^3 were used. Samples were sealed in evacuated quartz ampoules together with a sufficient amount of Zr sponge, which served as an oxygen getter. Samples were annealed at temperatures ranging from 600 to 1000 °C, and the annealing time was varied from 20 to 168 h. The ampoules were heated in a box furnace with a ramp rate of 10 °C/min and quenched in water at the end of the annealing time.

The samples were characterized by x-ray diffraction (at room temperature) using a Picker four-circle diffractometer with Cu $K\alpha$ radiation ($\lambda = 1.5418$ Å). Electrical characterization included resistivity and Hall measurements, from which the free carrier density in the SrTiO$_3$ crystals was determined. For resistivity measurements, the van der Pauw method was used. Resistance was measured at a current of 300 μA in the temperature range from 300 to 4 K. For the Hall coefficient measurements, square samples were cut into 5×1 mm^2 slabs, and contacts were attached on the sides of the slabs. On one of the long sides, two resistance bridges were attached in order to eliminate the residual voltage resulting from the lack of symmetry in the position of wires. The measurements were performed at 300 K. Magnetic sweep from −5000 to 5000 G was performed while passing a current of 0.1 A through the sample.

For the re-oxidation experiments, we used the SrTiO$_3$ samples reduced at 900 °C for 168 h following the procedure described above. Re-oxidation experiments were performed in a horizontal tube furnace in flowing ultrapure oxygen for 1 h. The re-oxidation was performed at temperatures from 200 to 500 °C.

Raman spectra were recorded using a SPEX Triplemate spectrometer equipped with a liquid-nitrogen-cooled multi-channel coupled-charge-device detector. The samples were attached to the cold finger inside a continuous He flow cryostat. Spectra were recorded in backscattering geometry in the temperature range 10–300 K. The 514.5 nm Ar$^+$ laser line was used for excitation.

III. RESULTS AND DISCUSSION

Figure 1 shows x-ray diffraction results for a SrTiO$_3$ sample reduced at 1000 °C for 20 h. As follows from the electrical characterization (below), it has high concentration of oxygen vacancies (free career concentration of 3.9 $\times 10^{19}$ cm^{-3}). The $\theta - 2\theta$ scan shows the same pattern as that of initial SrTiO$_3$ crystal, and the cubic lattice parameter de-
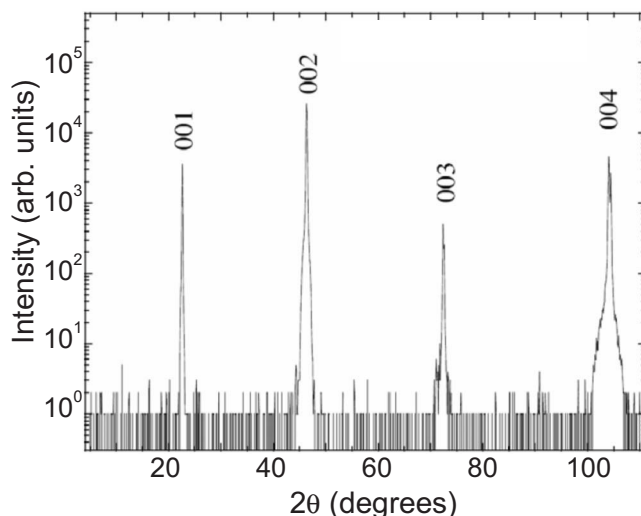
FIG. 1. X-ray diffraction pattern ($\theta - 2\theta$ scan) of SrTiO$_3$ sample 1000-20, reduced with Zr for 20 h at 1000 °C.

termined is 3.906 Å, which is the same as the bulk SrTiO$_3$ within the accuracy of the measurement. The x-ray diffraction results show that oxygen vacancies in the amounts introduced in our experiments do not cause any noticeable changes in the average crystal structure, which remains the same as in initial SrTiO$_3$ crystals. This result of the insensitivity of the lattice constant of SrTiO$_{3-x}$ to oxygen vacancies even for very large $x=0.5$ is in agreement with previous studies.[20–22] However, oxygen reduction causes significant changes in electrical and optical properties. Initial SrTiO$_3$ single crystal samples are optically transparent in the visible range and are insulating. After the reduction, they become black (absorbing) and conducting due to the presence of free charge carriers resulting from oxygen deficiency.

The reduction times and temperatures for the samples studied and their room temperature electrical resistivities and free career densities are given in Table I. Figure 2(a) shows the resistivity as a function of reduction time for the samples annealed at 900 °C. Resistivity as a function of temperature

TABLE I. Reduction parameters and room temperature electrical characteristics of the samples studied.

Sample number	Reduction temperature (°C)	Reduction time (h)	Conductivity at 295 K (Ω^{-1} cm^{-1})	Carrier density (cm^{-3})
900-20	900	20	7.5	7.80×10^{18}
900-36	900	36	66.7	4.17×10^{19}
900-48	900	48	76.9	
900-60	900	60	103.1	2.31×10^{20}
900-72	900	72	112.4	
900-168	900	168	156.0	2.40×10^{20}
600-20	600	20	3.8	
800-20	800	20	4.1	
1000-20	1000	20	65.2	3.91×10^{19}
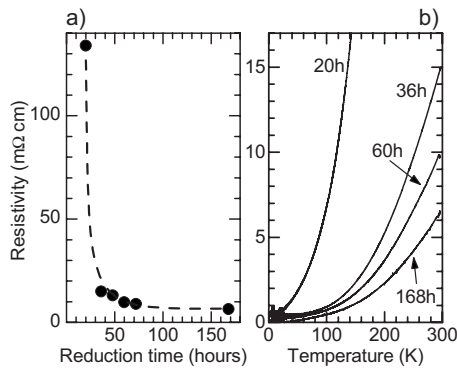
FIG. 2. (a) Resistivity as a function of reduction time for the samples reduced at 900 °C. (b) Temperature dependence of resistivity for this sample series. The curves are labeled by the reduction times in hours.

for these samples is shown in Fig. 2(b). Resistivity in all of the reduced $SrTiO_3$ samples decreases with temperature (metalliclike behavior). The concentration of oxygen vacancies was estimated using the free carrier density determined from the Hall measurements and assuming two free carriers for each oxygen vacancy, as has been previously reported.[23] [Although at very high vacancy concentrations (over 10^{21} cm^{-3}) the number of free electrons per vacancy may be reduced,[21] such high concentrations have not been achieved in our experiments.] Thus, the vacancy concentration can be obtained by dividing by 2 the numbers in the last column of Table I.

Figure 3 shows the low temperature (10 K) Raman spectra of $SrTiO_3$ samples reduced at 900 °C for 20–168 h. The spectra of an untreated single crystal and a 1-μm-thick $SrTiO_3$ film grown by pulsed laser deposition (PLD) on $SrTiO_3$ substrates covered by 0.35-μm-thick $SrRuO_3$ buffer layers are also given for comparison. The thin film structure and Raman spectra are the same as reported for similar samples by Xi and co-workers.[6,7] Bulk $SrTiO_3$ is paraelectric at all temperatures with centrosymmetric cubic perovskite structure $m3m$ above 105 K, and all the phonons are symmetry forbidden in the first-order Raman scattering. The spectrum of untreated $SrTiO_3$ crystal is dominated by second-order features. Also, the structural modes at 44, 144, and 445 cm^{-1} (labeled R in Fig. 3) are present in the Raman spectra below 105 K. These modes are due to the antiferrodistortive cubic-tetragonal phase transition, which involves the rotation of the Ti-O octahedra. The resulting tetragonal structure $4/mmm$ is still centrosymmetric and the fundamental $SrTiO_3$ phonons remain Raman inactive.

The following behaviors were observed with increasing the reduction time (hence the number of oxygen vacancies): (1) Structural modes at 44, 144, and 445 cm^{-1} are present in the Raman spectra even in the most heavily reduced samples. This indicates that the antiferrodistortive phase transition at 105 K still takes place, i.e., the reduced $SrTiO_3$ still maintains the basic structural and lattice dynamical properties of bulk $SrTiO_3$. (2) The intensity of the forbidden first-order Raman peaks labeled TO$_m$, LO$_m$ in Fig. 3 increases noticeably when the vacancy concentration becomes larger than 10^{19} cm^{-3}, indicating the breakdown of the inversion sym-
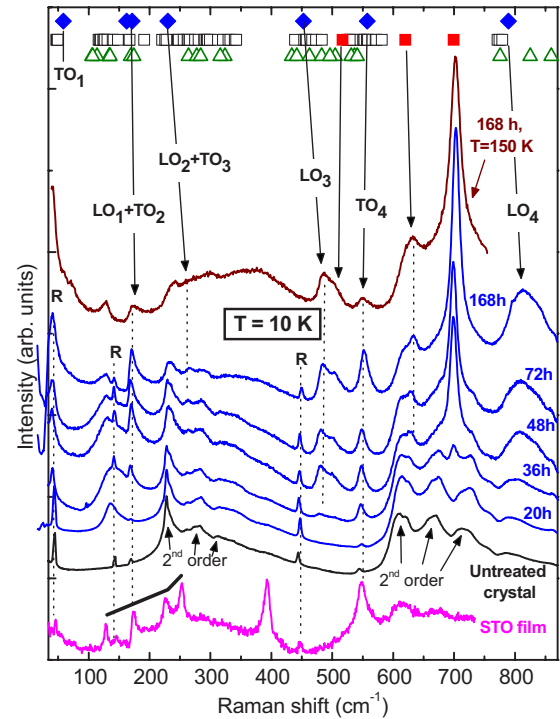
FIG. 3. (Color online) Raman spectra at $T=10$ K of a series of $SrTiO_3$ samples reduced at 900 °C in comparison with the spectrum of untreated crystal and $SrTiO_3$ film grown on $SrTiO_3$ substrate with $SrRuO_3$ buffer layer. Stars in the film spectrum indicate the $SrRuO_3$ lines. The results of the first-principles phonon calculations in the stoichiometric and oxygen-deficient $SrTiO_3$ crystals are shown by diamonds and squares, respectively. Triangles mark the calculated frequencies of the Brillouin-zone boundary (X, M, and R points) phonons in bulk $SrTiO_3$. Vertical dashed lines are guides for the eyes.

metry. (3) Several features appear in the spectra of reduced $SrTiO_3$ besides the first-order peaks of $SrTiO_3$ phonons. The feature at 135 cm^{-1} appears already in the sample with the smallest vacancy concentration. Additional features appear in the Raman spectra of reduced $SrTiO_3$ at about 505, 630, and 700 cm^{-1} at oxygen vacancy concentrations over 10^{19} cm^{-3}, and their intensity rapidly increases with vacancy concentration.

We attribute these new lines to the local vibrational modes associated with oxygen vacancies. A vacancy, being a point defect in the $SrTiO_3$ crystal lattice, changes the local potential configuration for the neighboring atoms, which causes them to vibrate at different frequencies compared to the perfect crystal. In order to estimate at what frequencies these local vibrational modes can appear, we performed a first-principles calculation of phonons in a cubic $SrTiO_3$ crystal with a neutral oxygen vacancy. A plane-wave density-functional theory based method[24] with ultrasoft pseudo-potentials[25] was utilized for the relaxation of ionic positions in a supercell, after which the phonon frequencies were computed with the help of a density-functional perturbation theory (DFPT) approach.[26] Local-density approximation (LDA) was used to account for exchange and correlations. The electronic wave function and density plane-wave cutoffs

TABLE II. Computed phonon frequencies ω (cm^{-1}) of cubic STO at k points Γ, X, M, and R. Symmetry labels follow the convention of Ref. 30.

Γ (0,0,0)		X $(\frac{1}{2},0,0)$		M $(\frac{1}{2},\frac{1}{2},0)$		R $(\frac{1}{2},\frac{1}{2},\frac{1}{2})$	
Label	ω	Label	ω	Label	ω	Label	ω
Γ_{15} (acoustic)	0	$X_{5'}$	106	M_3	26 i	R_{25}	89 i
Γ_{15} (TO)	59	X_5	135	$M_{2'}$	106	R_{15}	134
Γ_{15} (LO)	162	$X_{2'}$	169	$M_{5'}$	114	R_{15}	434
Γ_{15} (TO)	171	X_5	174	$M_{3'}$	134	$R_{25'}$	442
Γ_{25} (TO and LO)	230	X_3	278	$M_{5'}$	264	$R_{12'}$	505
Γ_{15} (LO)	453	X_1	284	M_5	324	$R_{2'}$	860
Γ_{15} (TO)	557	$X_{5'}$	316	M_1	463		
Γ_{15} (LO)	789	X_5	531	$M_{5'}$	482		
		X_1	541	$M_{3'}$	496		
		$X_{2'}$	776	M_2	536		
				M_4	825		

were 30 and 270 Ry, respectively. The vacancy was created by removing a single oxygen atom from a supercell containing eight unit cells of cubic SrTiO$_3$—with a theoretical lattice constant equal to 3.858 Å in this investigation—in a 2 $\times 2 \times 2$ configuration. A $4 \times 4 \times 4$ Monkhorst-Pack mesh[27] was employed for all the Brillouin-zone integrations, and the system was considered to be at equilibrium when the Hellman-Feynman forces on the ions were less than 0.5 $\times 10^{-3}$Ry/bohr. Due to the use of periodic boundary conditions, such a small supercell produces an ordered array of oxygen vacancies with a density significantly higher than that in our samples (4.2%, or 2×10^{21} cm^{-3}) and, as it has been recently shown, much larger supercells containing up to 320 atoms are required to accurately reproduce the electronic properties of oxygen vacancies at more realistic concentrations.[28] Because of the computational limitations, however, the larger supercells cannot currently be used for first-principles phonon calculations, which leaves the $2 \times 2 \times 2$ supercell as the only reference system that could be treated with DFPT-LDA methods, thus providing clues to how the vibrational spectrum of SrTiO$_3$ changes due to the presence of oxygen vacancies. We did not consider the possibility of formation of vacancy clusters because the concentration of vacancies in the samples measured is not very high and the cluster formation is unlikely. We should note that although our calculations were performed for the cubic phase of SrTiO$_3$, the spectra taken at $T=10$ K correspond to the tetragonal antiferrodistortive phase.[29] However, the antiferrodistortive phase transition at 105 K has no noticeable effect on the zone-center phonon modes, simply leading to the appearance of the R modes in the spectra. To illustrate this, a spectrum of SrTiO$_3$ sample reduced at 900 °C for 168 h measured at $T=150$ K is shown in Fig. 3 for comparison. As one can see, this spectrum contains all the same features as the spectrum measured at $T=10$ K except for the R modes.

The calculated phonon frequencies in oxygen-deficient SrTiO$_3$ are represented by squares in Fig. 3. These frequencies correspond to the zone-center optical phonons similar to those of a stoichiometric crystal as well as to the phonons

obtained by the folding of phonon branches of bulk SrTiO$_3$ (X, M, and R points corresponding to the rotations of oxygen octahedra, some of which can be seen in the spectra below the structural phase transition at 105 K) within the reduced Brillouin zone of the $2 \times 2 \times 2$ supercell. The phonon frequencies calculated for bulk stoichiometric SrTiO$_3$, which are presented in Table II, appear to be in good agreement with other reported calculations[31–33] and experimental neutron scattering results.[30,34] A comparison of calculated phonon frequencies for oxygen-deficient and stoichiometric SrTiO$_3$ shows that the oxygen-deficient SrTiO$_3$ possesses several vibrational modes at frequencies where the bulk phonon density of states is zero, in particular, 517, 620, and 699 cm^{-1}, shown in Fig. 3 by solid squares. These modes must be originating from the defects in the SrTiO$_3$ lattice, and their frequencies agree very well with the positions of the observed new lines in the Raman spectra. This supports the assignment of these peaks to the local vibrational modes associated with oxygen vacancies.

The feature around 135 cm^{-1} appears in reduced SrTiO$_3$ at significantly smaller vacancy concentrations than local vibrational modes discussed above, and it does not exhibit such a strong increase in intensity with increasing vacancy concentration. The origin of this feature is not clear. Soft TO$_1$ modes were reported in heavily reduced[19,35] and doped SrTiO$_3$ (Ref. 36) in this frequency range, but they exhibit different behavior. The position of the feature we observed is nearly independent of temperature and vacancy concentration, while the soft modes exhibit a characteristic temperature dependence and a significant hardening with increasing vacancy concentration.[19,35,36] A possible origin of this feature may be non-zone-center (e.g., acoustic) phonons activated by a structural disorder caused by oxygen vacancies. Disorder-activated phonons in Raman spectra are known in solids.[37,38] These modes generally reflect the phonon density of states. In SrTiO$_3$, according to calculations[33] the phonon density of states has the strongest maximum at about 120 cm^{-1}, which is close to the position of the observed feature. A spectral feature at close frequencies was also observed in
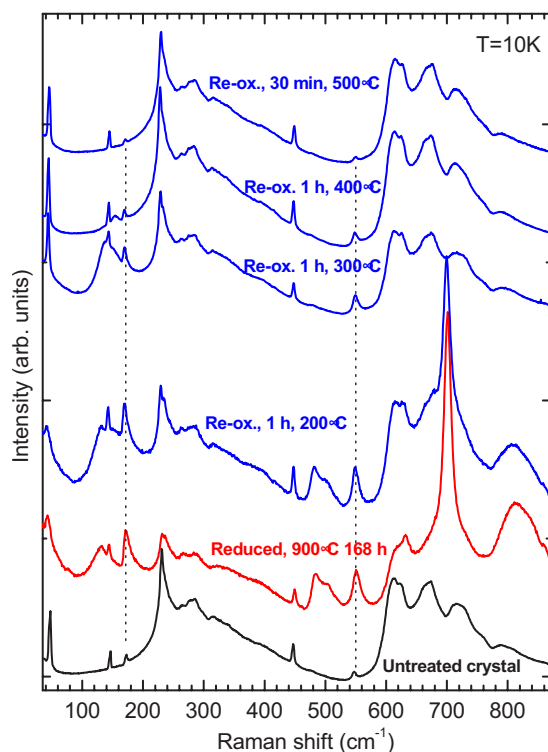
FIG. 4. (Color online) Raman spectra of $SrTiO_3$ samples reduced at 900 °C for 168 h and then re-oxidized by annealing in ultrapure oxygen for 1 h (except for the top spectrum annealed for 30 min at different temperatures). The spectra of untreated crystal and reduced sample before re-oxidation are given for comparison. Vertical dashed lines are guides for the eyes.

$Ba_xSr_{1-x}TiO_3$ and attributed to the disorder-activated Raman scattering in a solid solution.[39]

Figure 4 shows the spectra of $SrTiO_3$ samples reduced at 900 °C for 168 h and then re-oxidized for 1 h at different temperatures. As one can see, the re-oxidation of heavily reduced $SrTiO_3$ leads to complete restoration of the initial shape of Raman spectra. This demonstrates that the observed evolution of Raman spectra of reduced $SrTiO_3$ is indeed caused by oxygen vacancies.

Comparing the Raman spectra of reduced $SrTiO_3$ crystals and $SrTiO_3$ films grown by PLD, one can see that both in films and in reduced $SrTiO_3$ there are first-order peaks of $SrTiO_3$ phonons. This indicates that there are local regions where the inversion symmetry is broken, and $SrTiO_3$ phonons become Raman active. In reduced $SrTiO_3$, the oxygen vacancies, being polar defects, are responsible for the appearance of the polar regions. However, in reduced $SrTiO_3$ the first-order Raman peaks appear at rather high vacancy concentrations, where $SrTiO_3$ becomes conductive. The appearance of the first-order phonon lines is accompanied by the peaks of local vibrational modes associated with oxygen vacancies. The latter modes have not been observed in $SrTiO_3$ films, which are still insulating.[40] Therefore, we conclude that although oxygen vacancies do cause the formation of polar nanoregions, in thin films the vacancy concentration is not high enough to cause such intensive first-order Raman scattering. There must be another or additional cause for po-

lar regions in $SrTiO_3$ films. Polar impurities may lead to similar effects, but very high doping levels are needed (tenths of percent) to induce a significant first-order Raman scattering,[41,42] which is unlikely in nominally undoped films we studied. Sr/Ti nonstoichiometry could be another possible factor, but it is difficult to prove the existence of a small amount of nonstoichiometry in thin films.

Strain in thin epitaxial films can be an important factor strongly affecting their properties.[43] Transmission electron microscopy (TEM) studies were performed on $SrTiO_3/SrRuO_3$ epitaxial bilayers grown on $LaAlO_3$ substrates,[15] which Raman spectra are similar to those of $SrTiO_3/SrRuO_3$ films on $SrTiO_3$ shown in Fig. 3. TEM results demonstrate that the lattice mismatch between the substrate and the $SrRuO_3$ layer is mostly relaxed by dislocations in the vicinity of the $SrRuO_3$/substrate interface, although some defects propagate through the $SrRuO_3$ layer and reach the $SrRuO_3/SrTiO_3$ interface, resulting in defects in the $SrTiO_3$ layers.[15] The lattice mismatch between $SrRuO_3$ and $SrTiO_3$ (0.64%) is small compared to that between $SrRuO_3$ and $LaAlO_3$ (3.6%); therefore, one can expect a significantly smaller dislocation density in $SrTiO_3/SrRuO_3$ films on $SrTiO_3$ substrates compared to the films on $LaAlO_3$. However, Raman spectra are similar for the films grown on $SrTiO_3$ and $LaAlO_3$ substrates, both showing the forbidden first-order Raman peaks. Therefore, we believe that dislocations are unlikely to cause the observed features in the Raman spectra.

The small misfit between the $SrRuO_3$ layer and the $SrTiO_3$ film was shown to be mainly not relaxed and accommodated by elastic strain in the $SrTiO_3$ films.[15] A uniform uniaxial strain does not, however, break the inversion symmetry and cannot cause the observed Raman peaks in the films, unless the strain exceeds the critical value for inducing ferroelectricity,[44] which is not the case in our films. Although we cannot rule out the influence of the inhomogeneous strain distribution in the films, we believe that the likely cause for the appearance of polar nanoregions is the dipoles localized at the grain boundaries in films. The polar grain boundaries were proposed by Petzelt *et al.*[16] to explain the observed soft mode hardening and the appearance of the first-order Raman peaks of considerable intensity in $SrTiO_3$ ceramics. The ceramics studied were nominally pure, highly stoichiometric, and not subject to strain, yet the first-order Raman peaks were observed. Ostapchuk *et al.*[14] studied polycrystalline $SrTiO_3$ films and also observed the activation of the forbidden modes in the Raman spectra in the whole temperature range studied (80–300 K), which was explained by the dipoles associated with such defects as porosity and cracks along the grain boundaries. Although these defects were not found in epitaxial films studied here, the dipoles frozen at the grain boundaries can still exist and induce the polar phase in the bulk of grains, leading to the symmetry breakdown and the appearance of the forbidden modes in the Raman spectra.

IV. SUMMARY

Raman studies of reduced $SrTiO_3$ crystals demonstrated that oxygen vacancies do cause the symmetry breakdown

and the appearance of the first-order Raman peaks. Oxygen reduction also leads to the appearance of local vibrational modes associated with vacancies the in the Raman spectra. Observed significant differences in the lattice dynamical behavior of reduced $SrTiO_3$ crystals and thin films indicate the importance of other factors such as polar grain boundaries in determining the lattice dynamical properties of ferroelectric oxide films.

*Electronic address: dmitritenne@boisestate.edu

†Present address: Materials Science Division, Argonne National Laboratory, Argonne, IL 60439, USA.

[1] M. E. Lines and A. M. Glass, *Principles and Applications of Ferroelectrics and Related Materials* (Oxford University Press, New York, 1977).

[2] *Thin Film Ferroelectric Materials and Devices*, edited by R. Ramesh (Kluwer Academic, Boston, 1997).

[3] R. Ramesh, S. Aggarwal, and O. Auciello, Mater. Sci. Eng., R. **32**, 191 (2001).

[4] M. Dawber, K. M. Rabe, and J. F. Scott, Rev. Mod. Phys. **77**, 1083 (2005).

[5] A. A. Sirenko, C. Bernhard, A. Golnik, Anna M. Clark, Jianhua Hao, Weidong Si, and X. X. Xi, Nature (London) **404**, 373 (2000).

[6] A. A. Sirenko, I. A. Akimov, J. R. Fox, A. M. Clark, Hong-Cheng Li, Weidong Si, and X. X. Xi, Phys. Rev. Lett. **82**, 4500 (1999).

[7] I. A. Akimov, A. A. Sirenko, A. M. Clark, J.-H. Hao, and X. X. Xi, Phys. Rev. Lett. **84**, 4625 (2000).

[8] D. A. Tenne, A. Soukiassian, M. H. Zhu, A. M. Clark, X. X. Xi, H. Choosuwan, Qi He, R. Guo, and A. S. Bhalla, Phys. Rev. B **67**, 012302 (2003).

[9] D. A. Tenne, A. Soukiassian, X. X. Xi, H. Choosuwan, R. Guo, and A. S. Bhalla, J. Appl. Phys. **96**, 6597 (2004).

[10] Yu. I. Yuzyuk, V. A. Alyoshin, I. N. Zakharchenko, E. V. Sviridov, A. Almeida, and M. R. Chaves, Phys. Rev. B **65**, 134107 (2002).

[11] Yu. I. Yuzyuk, P. Simon, I. N. Zakharchenko, V. A. Alyoshin, and E. V. Sviridov, Phys. Rev. B **66**, 052103 (2002).

[12] Yu. I. Yuzyuk, J. L. Sauvajol, P. Simon, V. L. Lorman, V. A. Alyoshin, I. N. Zakharchenko, and E. V. Sviridov, J. Appl. Phys. **93**, 9930 (2003).

[13] K. A. Müller and H. Burkard, Phys. Rev. B **19**, 3593 (1979).

[14] T. Ostapchuk, J. Petzelt, V. Železný, A. Pashkin, J. Pokorný, I. Drbohlav, R. Kužel, D. Rafaja, B. P. Gorshunov, M. Dressel, Ch. Ohly, S. Hoffmann-Eifert, and R. Waser, Phys. Rev. B **66**, 235406 (2002).

[15] J. C. Wu, C. L. Jia, K. Urban, J. H. Hao, and X. X. Xi, J. Appl. Phys. **89**, 5653 (2001); J. Mater. Res. **16**, 3443 (2001).

[16] J. Petzelt, T. Ostapchuk, I. Gregora, I. Rychetský, S. Hoffmann-Eifert, A. V. Pronin, Y. Yuzyuk, B. P. Gorshunov, S. Kamba, V. Bovtun, J. Pokorný, M. Savinov, V. Porokhonskyy, D. Rafaja, P. Vaněk, A. Almeida, M. R. Chaves, A. A. Volkov, M. Dressel, and R. Waser, Phys. Rev. B **64**, 184111 (2001).

[17] R. Waser and D. M. Smyth, in *Ferroelectric Thin Films: Synthesis and Basic Properties*, edited by C. P. de Araujo, J. F. Scott, and G. W. Taylor (Gordon and Breach, Amsterdam, 1996), p. 47.

[18] H. Uwe, H. Yamaguchi, and T. Sakudo, Ferroelectrics **96**, 123 (1989).

[19] D. A. Crandles, B. Nicholas, C. Dreher, C. C. Homes, A. W. McConnell, B. P. Clayman, W. H. Gong, and J. E. Greedan, Phys. Rev. B **59**, 12842 (1999).

[20] M. Kestigian, J. G. Dickinson, and R. Ward, J. Am. Chem. Soc. **79**, 5598 (1957).

[21] W. Gong, H. Yun, Y. B. Ning, J. E. Greedan, W. R. Datars, and C. V. Stager, J. Solid State Chem. **90**, 320 (1991).

[22] T. Ohnishi, M. Lippmaa, T. Yamamoto, S. Meguro, and H. Koinuma, Appl. Phys. Lett. **87**, 241919 (2005).

[23] H. Yamada and G. R. Miller, J. Solid State Chem. **6**, 169 (1973).

[24] We used the PWSCF code (available from http://www.pwscf. org) for the calculations presented here.

[25] D. Vanderbilt, Phys. Rev. B **41**, 7892 (1990).

[26] S. Baroni, S. de Gironcoli, A. Dal Corso, and P. Giannozzi, Rev. Mod. Phys. **73**, 515 (2001).

[27] H. J. Monkhorst and J. D. Pack, Phys. Rev. B **13**, 5188 (1976).

[28] J. P. Buban, H. Iddir, and S. Öğüt, Phys. Rev. B **69**, 180102(R) (2004); R. A. Evarestov, E. A. Kotomin, and Yu. F. Zhukovskii, Int. J. Quantum Chem. **106**, 2173 (2006).

[29] Detailed phonon calculations for the antiferrodistortive phase of $SrTiO_3$ are currently under way.

[30] R. A. Cowley, Phys. Rev. **134**, A981 (1964).

[31] W. Zhong, R. D. King-Smith, and D. Vanderbilt, Phys. Rev. Lett. **72**, 3618 (1994).

[32] C. Lasota, C.-Z. Wang, R. Yu, and H. Krakauer, Ferroelectrics **194**, 109 (1997).

[33] T. Trautmann and C. Falter, J. Phys.: Condens. Matter **16**, 5955 (2004).

[34] W. G. Stirling, J. Phys. C **5**, 2711 (1972).

[35] D. Bäuerle, D. Wagner, M. Wöhlecke, B. Dorner, and H. Kraxenberger, Z. Phys. B: Condens. Matter **38**, 335 (1980).

[36] F. Gervais, J.-L. Servoin, A. Baratoff, J. G. Bednorz, and G. Binnig, Phys. Rev. B **47**, 8187 (1993).

[37] P. Benassi, O. Pilla, V. Mazzacurati, M. Montagna, G. Ruocco, and G. Signorelli, Phys. Rev. B **44**, 11734 (1991).

[38] A. Ingale and K. C. Rustagi, Phys. Rev. B **58**, 7197 (1998).

[39] V. V. Lemanov, Phys. Solid State **39**, 318 (1997).

[40] H.-C. Li, W. D. Si, R.-L. Wang, Y. Xuan, B. T. Liu, and X. X. Xi, Mater. Sci. Eng., B **56**, 218 (1998).

[41] U. Bianchi, W. Kleemann, and J. G. Bednorz, J. Phys.: Condens. Matter **6**, 1229 (1994).

[42] V. Porokhonskyy, A. Pashkin, V. Bovtun, J. Petzelt, M. Savinov, P. Samoukhina, T. Ostapchuk, J. Pokorný, M. Avdeev, A. Kholkin, and P. Vilarinho, Phys. Rev. B **69**, 144104 (2004).

[43] J. H. Haeni, P. Irvin, W. Chang, R. Uecker, P. Reiche, Y. L. Li, S. Choudhury, W. Tian, M. E. Hawley, B. Craigo, A. K. Tagantsev, X. Q. Pan, S. K. Streiffer, L. Q. Chen, S. W. Kirchoefer, J. Levy, and D. G. Schlom, Nature (London) **430**, 758 (2004).

[44] Y. L. Li, S. Choudhury, J. H. Haeni, M. D. Biegalski, A. Vasude-varao, A. Sharan, H. Z. Ma, J. Levy, V. Gopalan, S. Trolier-McKinstry, D. G. Schlom, Q. X. Jia, and L. Q. Chen, Phys. Rev. B **73**, 184112 (2006).